J Infrared Milli Terahz Waves (2012) 33:1227–1238
DOI 10.1007/s10762-012-9938-2

Millimeter-wave Ground-based Synthetic Aperture Radar Imaging for Foreign Object Debris Detection: Experimental Studies at Short Ranges

Enes Yigit · Sevket Demirci · Atilla Unal · Caner Ozdemir · Alexey Vertiy

Received: 10 July 2012 / Accepted: 13 September 2012 /
Published online: 26 September 2012

Abstract In this paper, millimeter-wave imaging of foreign object debris (FOD)-type objects on the ground is studied with the help of ground-based synthetic aperture radar (GB-SAR) technique. To test the feasibility of detecting runway FODs with this technique, some preliminary experiments are conducted within short antenna-to-target ranges of small imaging patches. An automated stripmap GB-SAR system with stepped-frequency transmission is constructed together with a quasi-monostatic data collection operation. The imaging experiments for various braces and screws are then carried out by using *32–36 GHz* and *90–95 GHz* frequency bands of the millimeter-wave. Images reconstructed by a matched-filter based algorithm are analyzed to determine the proper system parameters for an efficient imaging and to comprehend the factors against a successful detection. Results demonstrate the capability of GB-SAR imaging in accurately locating these FOD-like targets under near-range operating conditions.

Keywords Ground-based SAR · FOD · Matched-filter algorithm

1 Introduction

Synthetic aperture radar (SAR) is an important remote sensing technique capable of generating high resolution images of stationary targets on the ground. As being counterpart of conventional SAR, ground-based SAR (GB-SAR) systems [1–8] have recently become popular because they are easier to implement, cheaper in hardware and faster in collecting the scattered field data. Additionally, GB-SAR systems have the ability to acquire well resolved images of ground patches of limited sizes. Some applications of GB-SAR imagery include unstable slope monitoring [6], environment watch [7], investigation of artificial structures and observation of mature grain fields [8]. Although most GB-SAR systems have been operated at microwave

E. Yigit (✉) · S. Demirci · C. Ozdemir
Mersin University, Mersin, Yenisehir, Turkey
e-mail: enesyigit81@hotmail.com

A. Unal · A. Vertiy
Institute, International Laboratory for High Tech. (ILHT), TUBITAK MRC, Gebze, Kocaeli, Turkey

frequency bands, new problems that require fine resolutions have led the use of millimeter-wave (MMW) radiation in such applications [9, 10]. Evaluation of target/background signatures [11] and terrain remote sensing [12, 13] are some examples of these applications.

Among many MMW detection applications, detecting and removing foreign object debris (FOD) on airport runways has gathered an increasing attention after the crash of a Concorde jet in France in 2000 [14]. Consequently, many MMW detection applications have been studied by several researchers [15, 16]. Beasley et al. proposed a basic MMW radar circuitry to detect FODs on airport runways [15]. Although GB-SAR imaging technique seems also to have some potential; *it has not been exploited for removing FODs till now.* In this work, we aim to design, implement and apply GB-SAR imaging methodology such that we can do primary research towards the popular FOD detection application. For this purpose, after conceptually simulating the GB-SAR imaging problem, we have designed and constructed a MMW-band GB-SAR platform at the *International Laboratory for High Technologies (ILHT) of the Scientific and Technological Research Council of Turkey (TUBITAK) - Material Institute (MI)*. GB-SAR measurements were performed via the constructed experimental set-up. To test the imaging ability of the GB-SAR system, various numerical and experimental examples were realized. The results of our MMW GB-SAR implementations are presented and corresponding GB-SAR images were acquired by the help of the matched-filter algorithm (MFA).

The paper is organized as follows: In the next section, two-dimensional (2D) quasi-monostatic GB-SAR imaging system that uses stepped frequency continuous waveform (SFCW) is explained together with the formulation of the MFA. In the third section, an imaging simulation for perfect point targets is tried and the resultant GB-SAR image obtained by using MFA is demonstrated. In Section 4, the experimental set-up is explained and the conducted experiments are presented with their resultant GB-SAR images. In the concluding section, issues regarding the effectiveness of our approach for MMW GB-SAR based detection are discussed.

2 GB-SAR Imaging System

2D data collection geometry for a monostatic GB-SAR imaging is given in Fig. 1. As the radar antenna moves along a straight path, the scattered field data are gathered for various synthetic aperture point *y*. The 2D scattered electric field *S (f, y)* is recorded at different synthetic aperture locations and frequencies by the help of a SFCW radar system [17]. The radar measures the magnitude and phase of the received field for a range of distinct frequencies at each spatial point. For a particular position along the synthetic aperture, the backscattered signal *S (f, y)* can be represented as follows

$$S(f,y) = \iint \rho(x',y').e^{-j\frac{4\pi f}{c}\sqrt{(y-y')^2+x'^2}}dx'dy'. \quad (1)$$

where *c* is the speed of light and $\rho\ (x', y')$ is the scattering amplitude distribution within the illuminated SAR scene.

2.1 Imaging with MFA

One of the most critical steps in SAR data processing is to migrate the raw data such that a well focused SAR image can be formed. The MFA actually provides an optimal linear filter to maximize the signal to noise ratio of the scattered wave in the presence of additive noise to the radar system [18]. We start with implementation of the MFA with the fact that the

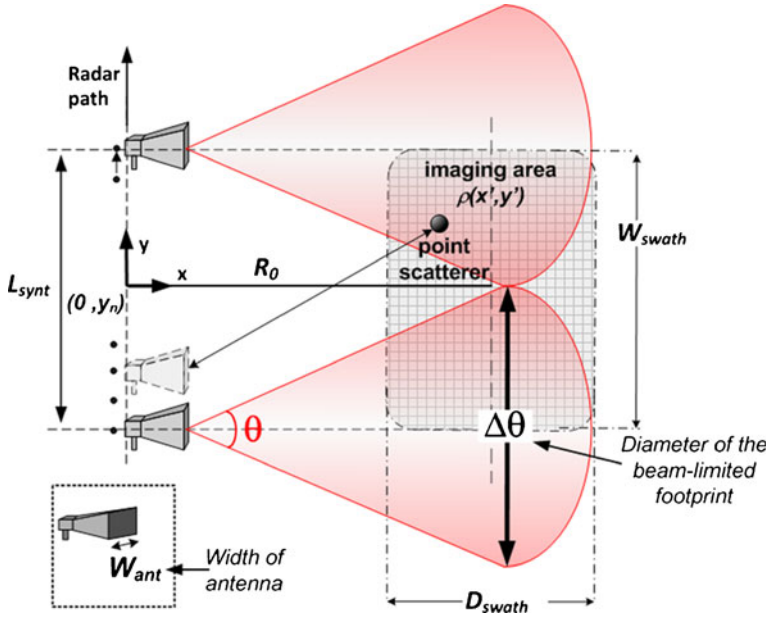

Fig. 1 2D data collection geometry for GB-SAR imaging

received backscattered field data from scatterers on the scene of GB-SAR system is given as shown in Eq. 1. The MFA basically states that [18] the optimal filter *H (f)* is the complex conjugate of the phase term in Eq. 1 as

$$\begin{aligned} H(f) &= K \cdot \left\{ e^{-j\frac{4\pi f}{c}\sqrt{(y-y')^2+x'^2}} \right\}^* \\ &= K \cdot e^{j\frac{4\pi f}{c}\sqrt{(y-y')^2+x'^2}} \end{aligned} \tag{2}$$

where K is a constant can be taken as 1 for simplicity without loss of generality. In reconstruction via MFA the measured SAR signal *S (f, y)* is correlated with this *H (f)* to give a measure of the reflectivity function; $\widehat{\rho}(x', y')$. Therefore, the MFA response can be written as given below [19]

$$\begin{aligned} \widehat{\rho}(x', y') &= \iint \{S(f, y)\} \cdot H(f) dy\, df \\ &= \iint \{S(f, y)\} \cdot e^{j\frac{4\pi f}{c}\sqrt{(y-y')^2+x'^2}} dy\, df \end{aligned} \tag{3}$$

It is worth noting to point out that the computational load of MFA is rather heavy due to the fact that the algorithm should calculate the integrals in Eq. 3 for every pixel in the resultant GB-SAR data.

2.2 Far-field Criteria

The distance of the target from the antenna and its extents is an important factor in radar signal processing algorithms. It is generally accepted that the target is in the far-field of the

antenna when the following conditions are met [20]

$$\begin{aligned} R_0 &\geq \tfrac{2W_{swath}}{\lambda} \\ R_0 &\approx 8.7 D_{swath} \end{aligned} \tag{4}$$

where R_0 is the range distance of the target from the radar path, D_{swath} and W_{swath} are the scene's range extent (or swath width) and cross-range extent (or swath length), respectively as demonstrated in Fig. 1. Obviously, far-field approximation has advantageous properties such as phase front uniformity and amplitude independency. But, when these conditions are not satisfied, the planar wavefront assumption will not be valid and hence the solution of the radar equations becomes more difficult. For such cases, the image reconstruction algorithms should assume spherical wave propagation in their processing steps to tolerate the resulted range migration effects. Since GB-SAR imaging applications such as FOD detection mostly operate within short ranges; a near-field algorithm should be used in these applications. We have exploited, therefore, the MFA that is inherently a near-field algorithm to achieve successfully focused imagery.

2.3 Resolutions

According to the SAR theory, the theoretical resolutions in range (δ_x) and cross-range domains (δ_y) can be calculated by [18, 21]

$$\begin{aligned} \delta_x &= \tfrac{c}{2B} \\ \delta_y &= \left\{ \begin{array}{ll} W_{ant}/2 & L_{synt} \geq \Delta\theta \\ R_0 \frac{\lambda_c}{2L_{synt}} & else \end{array} \right\} \end{aligned} \tag{5}$$

where B is the bandwidth of the incident wave, W_{ant} is an antenna width, $\Delta\theta$ is the diameter of the beam-limited footprint on the ground surface, λ_c is the carrier wavelength and L_{synt} is the synthetic aperture length of SAR as illustrated in Fig. 1.

2.4 Sampling Requirements

Another consideration for an effective imaging is the selection of sampling intervals in both frequency and spatial measurement directions. The maximum allowable sampling intervals for an alias-free imaging are calculated according to the Nyquist sampling criteria which are given as [20],

$$\begin{aligned} \Delta f &\leq \tfrac{c}{2R_{max}} \\ \Delta y &\leq \tfrac{\lambda_c}{2L_{synt}} \end{aligned} \tag{6}$$

where Δf is the frequency step, and R_{max} is the maximum range of imaging, Δy is the synthetic aperture step.

3 GB-SAR Simulation Example

Instead of directly stepping into real experiments, above mentioned GB-SAR geometry assumption was first tested with an imaging simulation example and by applying the MFA for the proof of the concept. Considering the 2D GB-SAR set-up shown in Fig. 2, a simulation in Matlab© programming language environment was carried out. The point

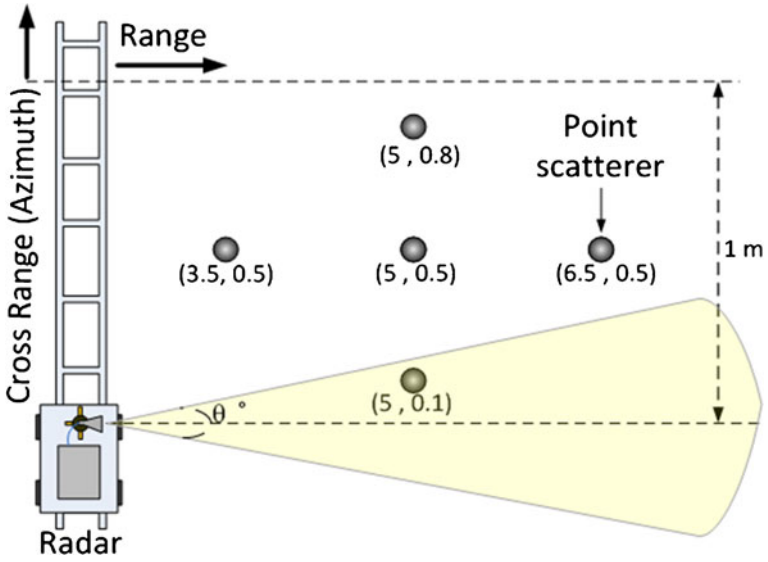

Fig. 2 GB-SAR imaging system geometry for the simulation

targets in the geometry were taken as perfect point scatterers of identical electromagnetic reflectivities. During the simulation, the following parameters were used: The backscattered field data were collected along a straight path ranging from *0 to 1 m* for a total of *501* evenly-spaced spatial points. The frequency was altered from *90 to 95 GHz* for a total of *251* uniformly spaced frequency points. Therefore, a *501* -by- *251* 2D spatial-frequency B-scan GB-SAR data were collected. After applying the MFA-based SAR focusing implementation, the radar image is obtained as shown in Fig. 3a. As it can be seen from the figure, the point scatterers are almost perfectly pinpointed at their true range and cross-range locations.

To comprehend the success of the focusing ability of the MFA, theoretical resolutions are calculated according to formulas given in Eq. 5. With current parameters of this simulation, they are calculated as *3 cm* and *0.81 cm* for range and cross-range domains, respectively. To measure the resolutions from the simulated image, the *−4.0 dB* contour line of a single scatterer located at *(y=0.5 m, x=5 m)* is extracted as shown in Fig. 3b. The corresponding *−4.0 dB* resolution values (that is approximately one Fourier bin) are measured to be *3.05 cm* and *0.83 cm* for the range and the cross-range resolutions, respectively. Therefore, the perfect match between the theoretical and the simulated resolutions clearly validates the precision of our MFA implementation for the GB-SAR problem.

4 GB-SAR Experiments

To be able to perform the MMW-band SAR measurements, the experimental setup shown in Fig. 4 was designed and constructed at the *ILHT* of *TUBITAK-MI*. The setup consists of a vector network analyzer (VNA), antennas, a rail-scanner, and a control computer. Two different VNAs both of which uses SFCW transmission were exploited throughout the experiments: one is operating within the *26.5 ~ 40 GHz* and the other is operating within the *90 ~ 140 GHz* bandwidth. The pyramidal horn type antennas that have half-power beam widths of approximately *12°* at *100 GHz* were used in the quasi-monostatic mode operation.

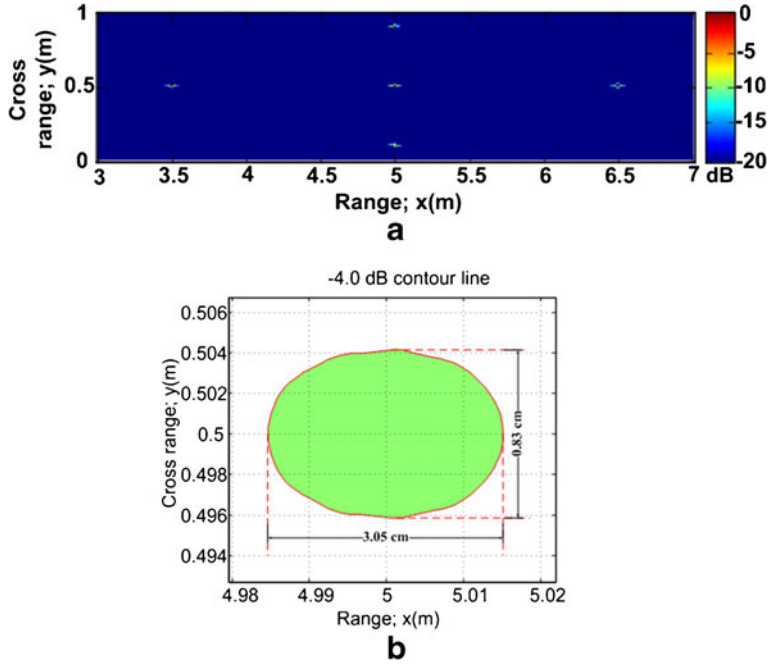

Fig. 3 GB-SAR imaging results for the simulation example: (**a**) Simulated MMW-band image (**b**) *-4.0 dB* contour line of the reconstructed image around the scatterer located at *(y=0.5 m, x=5 m)*

The rail-scanner, on which all the measurement equipments were put, has the ability to move the radar back and forth directions with high precision step increments. Synchronization between the rail-scanner and the VNA were completely automated by using the control computer and all of the measurements were done in a MMW semi-anechoic chamber facility.

To assess the use of SAR imaging principle for the MMW detection of FOD-type targets, two different preliminary experiments were conducted as explained in the following sections. In these experiments, very small patches of the ground and also very short antenna-to-

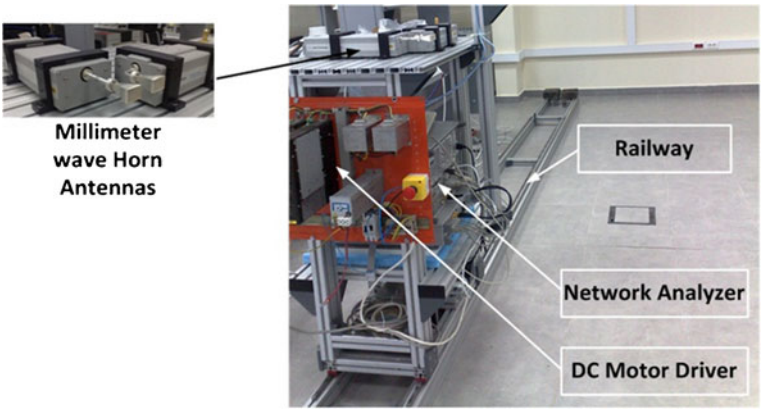

Fig. 4 The photo of the experimental GB-SAR platform with MMW-band horn antennas

ground operating distances (w.r.t. real runway dimensions) were considered together with appropriate orientations of the illumination. It is beneficial to note that this choice of the experimental configuration does not put any limit on our testing purpose of GB-SAR imaging for its use in a real application; since the concept will be identical for both cases. However, in a real FOD detection application, the distance of the antenna platform from the runway and its height from the ground, the beam pattern of the antennas, the desired imaging area on the runway, the corresponding sampling intervals in range and cross-range measurement directions, power requirements, all should be considered and arranged according to the desired specifications.

4.1 Experiment 1: Imaging the Braces

In the first experiment, two identical aluminum braces were tried to be imaged by using our GB-SAR experimental set-up. The geometrical illustration of the experiment with dimensions of the investigated targets and their distances from the radar are depicted in Fig. 5a.

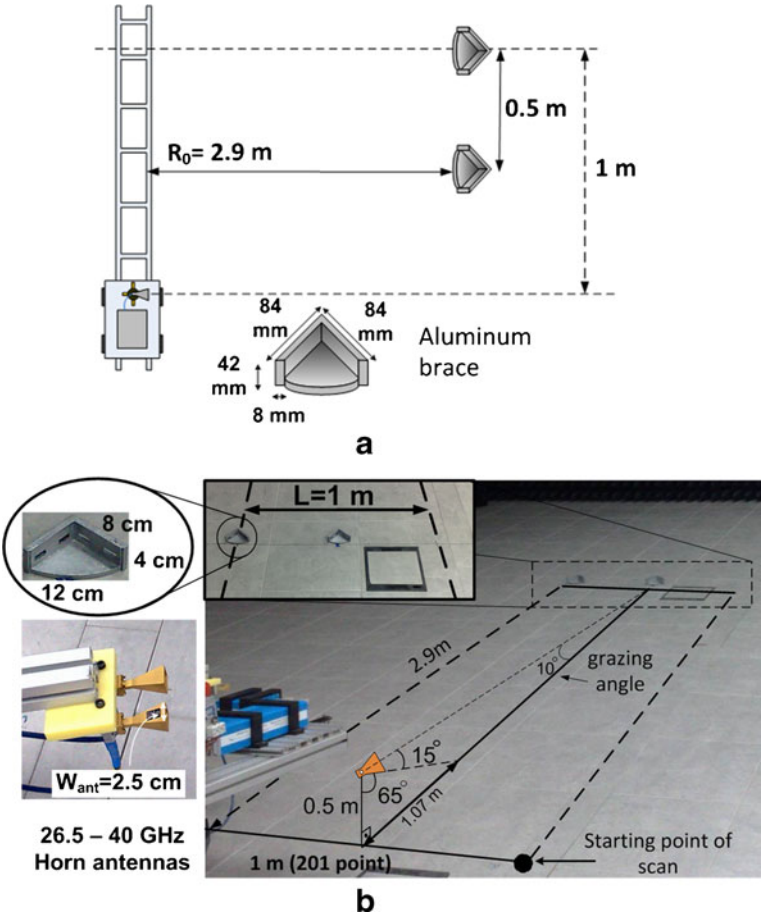

Fig. 5 Illustration of the first experiment: (**a**) geometrical representation, (**b**) photos of the braces and the measurement scene

The real experimental set-up and the antennas are shown in Fig. 5b in which the position of the radar and the targets can also be seen. The height of the antennas from the ground was set to *50 cm* and the look angle of the antennas whose azimuth beam width is about *23.6°* at *34 GHz*, was arranged as *80°*. Considering the sampling requirements given in Eq. 6, the length of the synthetic aperture was arranged to be *100 cm* to have *201* discrete measurement points and the frequency of the transmission was altered from *32 to 36 GHz* for a total of *201* distinct frequencies.

After collecting the backscattered field using the VNA, the raw data-set was fed to the MFA to be able to form a focused GB-SAR image. The resultant measured MMW-band GB-SAR image is shown in Fig. 6a. As obvious from the image, all targets are successfully imaged at their true locations with good image fidelities. The dominant scattering mechanism is shown to be occurred from the first aluminum brace (at the center of the synthetic aperture of $0 \sim 1\ m$) as expected. We also notice from the figure that reflections from the ground are still not shown within the dynamic range of $-30\ dB$ which indicates a clear detection of the investigated targets. This is due to the strong reflection characteristics of these targets that have corner structures and also the low grazing angle of the measurement *(10°)* that was adjusted according to the desired radar footprint illumination of this application. Based on the parameters used in this experiment, $\Delta\theta$ is calculated as *1.24 m* and the resolutions in range and cross-range domains are calculated as *3.75 cm* and *1.32 cm*, respectively. To obtain the resolutions from the measured data, the $-4.0\ dB$ contour line of the first target located at *(y=0.48 m, x=2.94 m)* is figured out as shown in Fig. 6b. The corresponding resolution values are found to be *3.78 cm* and *1.75 cm* for the range and cross-range resolutions, respectively.

4.2 Experiment 2: Imaging the Screws

The aim of this experiment was to investigate the detection capabilities of our GB-SAR imaging system for different metallic objects and also for the different carrier frequency usage. For this purpose, two identical screws were used in this case to be imaged within the W band of the MMW frequency range. The imaging geometry and the photos of the measured scene are shown in Fig. 7a and b, respectively. As it seen from Fig. 7a, the screws

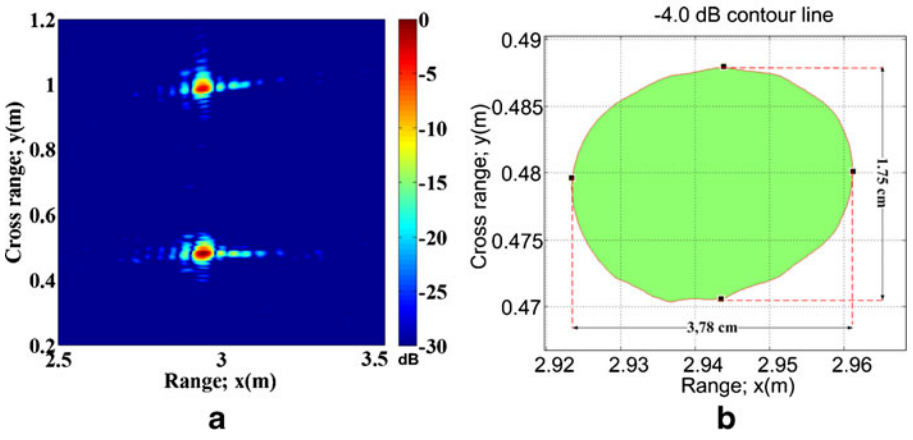

Fig. 6 GB-SAR imaging results for the first experiment: (**a**) measured MMW image (**b**) *-4.0 dB* contour line of the image around the scatterer located at *(y=0.48 m, x=2.94 m)*

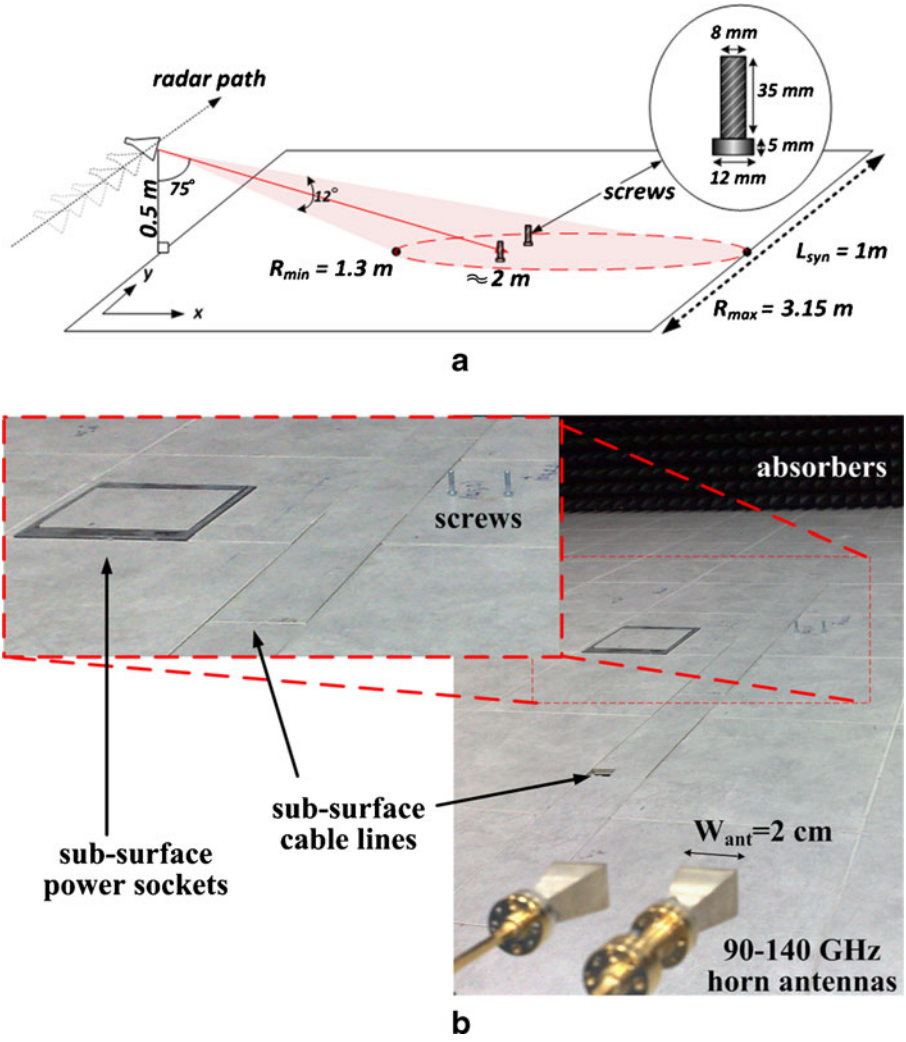

Fig. 7 Illustration of the second experiment: (**a**) geometrical representation, (**b**) photos of the screws and the measurement scene

were placed about *2 m* away from the antennas; but one of them was put *2 cm* closer than the other one. The spacing between the screws was set to *10 cm*. The height of the radar sensor was set again to *50 cm* but this time the look angle of the antennas whose azimuth half-power beamwidths are both *12.73°* at *92.5 GHz*, was arranged as *75°* to determine its effect on imaging. The length of synthetic aperture was *100 cm* for a total of *626* discrete measurement points and the frequency of the VNA was incremented with *50 MHz* steps ranging from *90 to 95 GHz* to have *101* distinct frequencies.

In this experiment, the backscattering data of the target-free background were also collected to exploit a background subtraction procedure which proved to be useful for increasing SNR. The resultant GB-SAR image without background process is shown in Fig. 8a. Since the RCS values of these screw targets are supposed to be lower than the braces

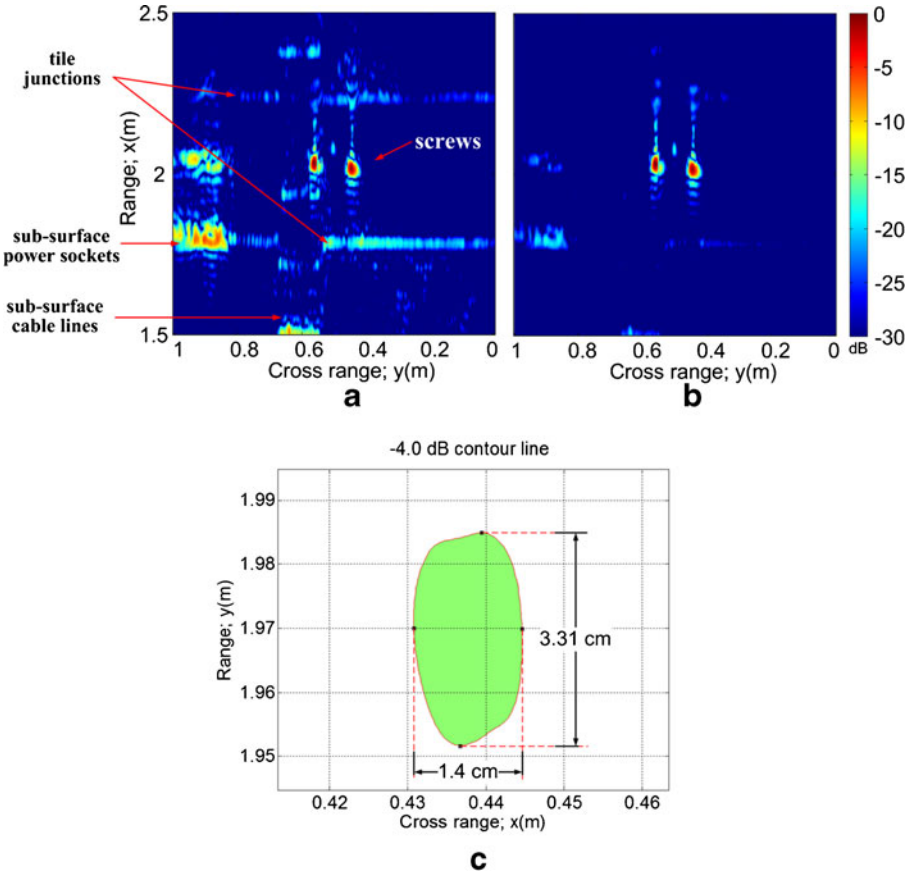

Fig. 8 GB-SAR imaging results for the second experiment. Measured MMW image: (**a**) without background subtraction (**b**) with background subtraction. (**c**) *-4.0 dB* contour line of the image around the scatterer located at *(y=0.44 m, x=1.97 m)*

and also the grazing angle of this illumination was higher than the first experiment, we see in this case, some strong scattering features from the background within the same dynamic range of imaging. These reflection energies result from the non-uniform structure of the investigated ground and it's beneath which comprise tile junctions, sub-surface power sockets and cable lines as visible in the photos of Fig. 7b. Despite these considerably strong clutter signals, the dominant scattering mechanisms in the GB-SAR image of Fig. 8a are shown to appear at the correct locations of the screws both in range and cross-range directions. To further enhance the detection performance, the background subtraction was applied to the acquired data and the image shown in Fig. 8b was obtained. We see from this image that the subtraction process suppresses almost all background signatures thereby providing a more clear detection of screw targets. For the selected bandwidth, range distance and synthetic aperture settings, the theoretical value for $\Delta\theta$ is calculated as *0.44 m* and the range and cross-range resolutions are found to be *3 cm* and *1 cm*, respectively. After the image is reconstructed, the values for range and cross-range resolutions are observed as *3.31 cm* and *1.4 cm* (see Fig. 8c) which are shown to be consistent with the theoretical values.

5 Conclusion

The main goal of this work was to provide a framework for the SAR imaging based detection of FODs on airport runways. For this aim, we have demonstrated the ground-based usage of SAR imagery to locate small metallic targets in the radiative near-field region. The results of the conducted experiments at the MMW-band frequencies have been presented. In all of these experiments, objects were accurately detected and imaged by the help of the precise implementation of the near-field image reconstruction algorithm. Therefore, the results in this work clearly demonstrate the capability of GB-SAR imagery in detecting small objects in the near-range operating distances.

We have observed from this study that the frequency band is more important when the high cross resolution is desired. While the range resolution depends on the bandwidth, center frequency plays a critical role in having a good cross range resolution. Therefore, to achieve a sharp cross-range resolution, high frequencies should be used. Furthermore, the look-angle choice is also important in the FOD detection task due to the possible strong reflections from the imaging ground and its surrounding. At the high squint angle positions, the multi-path effects become pronounced in the resulting image.

When a real application of FOD detection is considered by using the GB-SAR methodology, some modifications in the data collection geometry may be required to be able to use the system at an airport. This is due to the fact that while the conventional SAR systems generally works in the side-looking mode pointed perpendicular to the synthetic aperture path; a squint mode SAR employment has to be used if a variable azimuth imaging (i.e. runway) of the swath is desired. In the near future; therefore, we plan to further develop our GB-SAR system such that it can be adapted to any airport runway to fulfill this criterion.

References

1. L. Cazzani, C. Colesanti, D. Leva, G. Nesti, C. Prati, F. Rocca, and D. Tarchi, “A Ground-Based Parasitic SAR Experiment,” IEEE Trans. Geosci. Remote Sensing **38**(5), 2132–2141 (2000).
2. B. L. Cho, Y. K. Kong, H. G. Park and Y. S. Kim, “Automobile-Based SAR/InSAR System for Ground Experiments,” IEEE Trans. Geosci. Remote Sensing **3**(3), 401–405 (2006).
3. V. C. Koo, B. K. Chung, and H. T. Chuah, “Development of a ground-based radar for scattering measurements,” IEEE Antennas and Propagation Magazine **45**(2), 36–42 (2003).
4. M. Mohammad poor, R. S. A. Raja Abdullah, A. Ismail and A. F Abas, “A Circular Synthetic Aperture Radar For On-The-Ground Object Detection,” Progress In Electromagnetics Research **122**, 269–292, (2012)
5. K. S. Lim and V.C. Koo, “Design and Construction of Wideband VNA Ground-Based Radar System with Real and Synthetic Aperture Measurement Capabilities,” Progress In Electromagnetics Research, PIER **86**, 259–275 (2008)
6. M. Pieraccini, G. Luzi, D. Mecatti, L. Noferini and C. Atzeni, “Ground-based SAR for short and long term monitoring of unstable slopes,” Proceedings of the 3rd European Radar Conference, 92–95 (2006).
7. Z. S. Zhou, V. Boerner, and M. Sato, "Development of a Ground-Based Polarimetric Broadband SAR System for Non-Invasive Ground-truth Validation in Vegetation Monitoring,” IEEE Trans. Geoscience and Remote Sensing **42(**9), 1803–1810 (2004).
8. J. L. Gómez-Dans, S. Quegan and J. C. Bennett, “Indoor C-Band Polarimetric Interferometry Observations of a Mature Wheat Canopy,” IEEE Trans. Geosci. Remote Sensing **44**(4), 768–777 (2006).
9. Z. Wang, Q. Lai, R. Xu, B. Yan, W. Lin, and Y. Guo, “A Millimeter-Wave Ultra-Wideband Four-Way Switch Filter Module Based on Novel Three-Line Microstrip Structure Band-Pass Filters,” Progress In Electromagnetics Research, PIER **94**, 297–309 (2009).
10. E. Helmut, W. Alfred, S. Rainer and J. Winfried, “Ground based Millimeterwave SAR for the evaluation of Target- /Background Signatures,” Synthetic Aperture Radar (EUSAR), 2010 8th European Conference, 634–637 (2010).

11. E. Yiğit, A. Ünal, A. Kaya, Ş. Demirci, H. Çetinkaya, C. Özdemir and A. Vertiy, "Millimeter-Wave Ground Based Synthetic Aperture Radar Measurements", URSI General Assembly and Scientific Symposium, Istanbul, F05-2, 13–20, (2011)
12. G. Wadge, D.G. Macfarlane, D.A. Robertson, A.J. Hale, H. Pinkerton, R.V. Burrell, G.E. Norton, and M.R. James, "AVTIS: a novel millimetre-wave ground based instrument for volcano remote sensing", Journal of Volcanology and Geothermal Research **146**(4), 307–318 (2005).
13. R. Wellman, G. Goldman, J. Silvious, and D. Hutchins, *Analyses of Millimeter Wave Radar Low-Angle Ground-Clutter Measurements for European-Like and Desert Environments*, Army Research Laboratory - TR- 1102 (1996).
14. http://www.nytimes.com/2010/12/07/world/europe/07concorde.html (accessed in June 1st, 2012).
15. S.P Beasly, G. Binns, R. Hodges, R.J Badley, Tarsier., "A Millimetre Wave Radar for Airport Runway Debris Detection", in Proc. of EURAD'04, (2004), Amsterdam.
16. NAVTECH, http://www.nav-tech.com/Runway%20Surveillance.htm (accessed in June 1st, 2012).
17. T. Wu, X. Tang and F. Xiao, "Design of a W-band Stepped-frequency Synthesizer with Fast Frequency Switching," J Infrared Milli Terahz Waves **30,** 826–834 (2009).
18. C. Ozdemir, *Inverse Synthetic Aperture Radar Imaging With Matlab Algorithms* , A John Wiley & Sons, Inc., Publication (2012).
19. L. A. Gorham and L. J. Moore, "SAR image formation toolbox for MATLAB," E. G. Zelnio and F. D. Garber, Eds. **7699**(1). SPIE (2010).
20. E. J. Luminati, "Wide-Angle Multistatic Synthetic Aperture Radar: Focused Image Formation and Aliasing Artifact Mitigation" Master's thesis, air force inst of tech wright-patterson afb oh school of engineering and management (2005)
21. W. Wang, "Analysis of Waveform Errors in Millimeter-Wave LFMCW Synthetic Aperture Radar," Int J Infrared Milli Waves **27**, 1433–1444 (2006).